

## Bi<sub>2</sub>Te<sub>3</sub>–Te nanocomposite formed by epitaxial growth of Bi<sub>2</sub>Te<sub>3</sub> sheets on Te rod

Yuan Deng<sup>a,\*</sup>, Chang-Wei Cui<sup>a</sup>, Ni-La Zhang<sup>b</sup>, Tian-Hao Ji<sup>a</sup>, Qing-Lin Yang<sup>a</sup>, Lin Guo<sup>a</sup>

<sup>a</sup>*School of Materials Science & Engineering, Beijing University of Aeronautics & Astronautics, Beijing 100083, China*

<sup>b</sup>*Department of Physics, Tsinghua University, Beijing 100084, China*

Received 13 December 2005; received in revised form 9 February 2006; accepted 12 February 2006

Available online 20 March 2006

### Abstract

Single-crystal Bi<sub>2</sub>Te<sub>3</sub>–Te nanocomposites with heterostructure were synthesized using a two-step solvothermal process in the presence of ethylenediaminetetraacetic acid disodium salt. The first step is the formation of the Te nanorods and the second step is to grow the Bi<sub>2</sub>Te<sub>3</sub> sheets off the Te rods surface to form the Bi<sub>2</sub>Te<sub>3</sub>–Te nanocomposites. The products were characterized by X-ray diffraction, scanning electron microscopy and transmission electron microscopy. We demonstrate a method of an epitaxial growth of Bi<sub>2</sub>Te<sub>3</sub> nanosheets perpendicular to the axis of the central Te rod and a formation process of Bi<sub>2</sub>Te<sub>3</sub>–Te nanocomposites is also proposed.  
© 2006 Elsevier Inc. All rights reserved.

*Keywords:* Low-dimensional structures; Single crystal growth; Nanomaterials

### 1. Introduction

The performance of thermoelectric (TE) materials depends on the figure of merit  $ZT$  of the material ( $ZT = (\alpha^2 T / \rho \kappa)$ , where  $\alpha$  is the Seebeck coefficient,  $\rho$  is the electrical resistivity,  $\kappa$  is the thermal conductivity, and  $T$  is the absolute temperature). Currently, the bulk material with the highest thermoelectric figure of merit at room temperature (300 K) is Bi<sub>2</sub>Te<sub>3</sub> with  $Z = 0.003$ , but an improvement by about a factor of 2 is necessary for thermoelectric devices to be competitive with vapor-compression technology. Excellent TE materials require a perfect combination of electrical and thermal properties, which need achieve simultaneously high power factor ( $\alpha^2 / \rho$ ) and low thermal conductivity. Interests are then focused on searching for novel and more efficient TE for cooling and power generation applications. Hicks and Dresselhaus [1,2] pointed out that, it may be possible to increase  $Z$  of certain materials by a factor of several times of their bulk values if they have a 1D or 2D nanostructure. Thermoelectric properties of low-dimensional structures started to attract

attention in the 1990s. Impressive  $ZT$  values have been reported in some low-dimensional structures [3–5]. As bismuth telluride and its alloys are one of the best TE with the highest figure of merit  $Z$ , it is promising to enhance the overall TE properties by preparing nanostructured Bi<sub>2</sub>Te<sub>3</sub> materials or multicomposite [6–8].

Pure Bi<sub>2</sub>Te<sub>3</sub> materials with different shapes have been extensively developed by hard templates approach, kinetic control solution growth, and self-assembly [9–15] process, while nanocomposites with heterostructure are seldom reported. The challenges in this field are still the development of synthetic methods, control of morphology, and assembly of desired nanostructures. In previous work, we have reported controllable solvothermal growth of Bi<sub>2</sub>Te<sub>3</sub> sheet-rod by the oriented attachment of Bi<sub>2</sub>Te<sub>3</sub> sheets in the presence of ethylenediaminetetraacetic acid disodium salt (EDTA) [14]. This solvothermal method combining with the self-assembly techniques would be a promising method to synthesize crystalline nanostructural composites. Besides, the use of multi-dentate ligands instead of surfactants will make it possible to gain a new generation of sophisticated nanostructures.

Herein, a two-step solvothermal process was developed to prepare Bi<sub>2</sub>Te<sub>3</sub>–Te nanocomposites with

\*Corresponding author. Fax: +86 10 82338162.

E-mail address: [dengyuan@buaa.edu.cn](mailto:dengyuan@buaa.edu.cn) (Y. Deng).

heterostructure. We demonstrate an epitaxial growth of  $\text{Bi}_2\text{Te}_3$  nanosheets perpendicular to the axis of the central Te rod and a formation process of  $\text{Bi}_2\text{Te}_3$ -Te nanocomposites is also proposed. Low-dimensional Te nanorods and  $\text{Bi}_2\text{Te}_3$  sheets might reduce the lattice thermal conductivity further due to the phonon blocking effect of their low-dimensional nature. These structures enable the  $\text{Bi}_2\text{Te}_3$ -Te sheet-rods to be a potential TE material with a high figure of merit. The formation mechanism was also studied in detail.

## 2. Experimental

All chemicals were purchased from Beijing Chemical Co. Limited. Tellurium powders (99.99%, 0.191 g, 1.5 mmol) were put into a 50 ml Teflon-lined autoclave. The autoclave was then filled with *N,N*-dimethylformamide (DMF) up to 80% of its capacity, and KOH (2.225 g, 40 mmol) was added slowly into the autoclave and stirred for 0.5 h at room temperature. The autoclave was maintained at 180 °C for 2 h, followed by quick cooling in water to room temperature.  $\text{BiCl}_3$  (0.315 g, 1 mmol) and EDTA (0.744 g, 2 mmol) were added into cooled autoclave and stirred for 1 h. The autoclave was kept at 180 °C for another 4–30 h and then cooled to room temperature naturally. The products were filtered and washed with distilled water and absolute ethanol in sequence. Finally, the dark products were dried at 80 °C.

Powder X-ray diffraction (XRD) data were collected on a Rigaku D/MAX 2200 PC Automatic X-ray Diffractometer with  $\text{CuK}\alpha$  radiation ( $\lambda = 0.154056$  nm). The grain morphology and size were observed by scanning electron microscopy (SEM) (FEI Siron 200) and transmission electron microscopy (TEM) (HITACHI H-8100). Further structural and elemental analyses were performed using HRTEM (FEI Company, Tecnai G2 F20 S-Twin FEG TEM at 300 kV) and selected area electron diffraction (SAED).

## 3. Results and discussion

Fig. 1a shows the XRD patterns of the  $\text{Bi}_2\text{Te}_3$ -Te nanocomposite prepared at 180 °C for 20 h. It is identified as a mixture of rhombohedral  $\text{Bi}_2\text{Te}_3$  (shown in Fig. 1b) and hexagonal Te (JCPDS 36-1452). It is clear from the XRD pattern that the lattice spacing of our  $\text{Bi}_2\text{Te}_3$  and Te match closely to those of the bulk  $\text{Bi}_2\text{Te}_3$  and Te. The obtained lattice parameters for  $\text{Bi}_2\text{Te}_3$  are  $a = 4.38$  Å and  $c = 30.50$  Å, which are in agreement with the reported values  $a = 4.385$  Å,  $c = 30.48$  Å (JCPDS 15-0863). The intensity of Te peaks are nearly similar in relation to that of  $\text{Bi}_2\text{Te}_3$  peaks, which shows that no Te or  $\text{Bi}_2\text{Te}_3$  is dominant in the composites.

Under the two-step solvothermal treatment, Te powders reacted with  $\text{BiCl}_3$  to produce  $\text{Bi}_2\text{Te}_3$  sheets and  $\text{Bi}_2\text{Te}_3$ -Te sheet-rod-like materials. While we have not yet achieved 100%  $\text{Bi}_2\text{Te}_3$ -Te sheet-rods, only about 40% sheet-rods

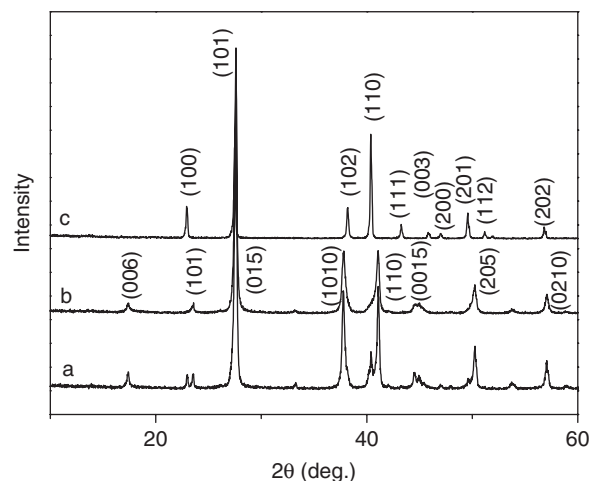


Fig. 1. XRD patterns of (a) the final product prepared at 180 °C for 20 h; (b)  $\text{Bi}_2\text{Te}_3$  particles prepared by the published solvothermal method [14]; (c) Te rods obtained at the first stage of the solvothermal process.

were found in the product. The SEM images of the sheet-rod-like materials are shown in Fig. 2. The sheet-rods are 300–500 nm in diameter and above several micrometers in length (shown in Figs. 2a and b). The nanosheets have grown on the surface of rod with the plane perpendicular to the axial direction of the rod. The thickness of the hexagonal plates ranges from more than 50–100 nm. The platelets grow out of a rod and they are mostly attached to the edge of a main body. The local chemical composition and crystallographic relationship between the nanoplatelets and rod have been analyzed by energy dispersive X-ray (EDX) analysis (shown in Fig. 2b inset), which indicates that the atomic composition ratio of Bi/Te in the sheets is about 2.02:3.10, in good agreement with that of the stoichiometric composition of  $\text{Bi}_2\text{Te}_3$ . Unlike that of the nanoplatelets, the content of Bi in the rod is so low that can be neglected, indicating that the major composition of the rod is Te and the platelets are made of  $\text{Bi}_2\text{Te}_3$  compound. Size control of the  $\text{Bi}_2\text{Te}_3$ -Te sheet-rods was achieved by adjusting the growth temperature and the growth time.

The sheet-rod-like structures of  $\text{Bi}_2\text{Te}_3$ -Te nanocomposites were further examined using TEM and HRTEM. TEM image as shown in Figs. 3a and b present the ordered and aligned arrangement among the platelets, which suggests a possible crystallographic orientation relationship among them. The selected area electron diffraction (SAED) pattern (inset in Fig. 3a) taken from a single sheet-rod indicates that the sheet-rods are single crystals. It is noticed that the SAED spots are not continuous but composed of discrete spots, which suggests preferential orientations of the  $\text{Bi}_2\text{Te}_3$  nanosheets in the Te rod. Figs. 3c–d are representative HRTEM images of a single-crystalline  $\text{Bi}_2\text{Te}_3$ -Te sheet-rod, which were acquired from the circled areas of A and B in Fig. 3b, respectively. These HRTEM images indicate an interesting phenomenon that the lattice planes in the  $\text{Bi}_2\text{Te}_3$  sheets have almost the same direction with the Te rod, and no apparent boundary is

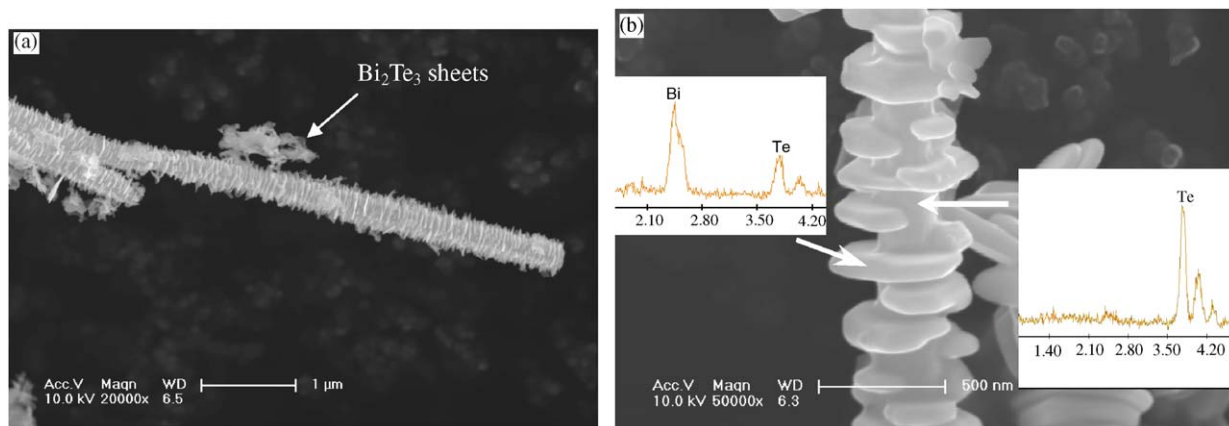


Fig. 2. SEM images of the resulting products (a) individual sheet-rods; (b) an individual sheet-rod with EDX patterns (inset) taken from sheet and rod, indicated by arrows.

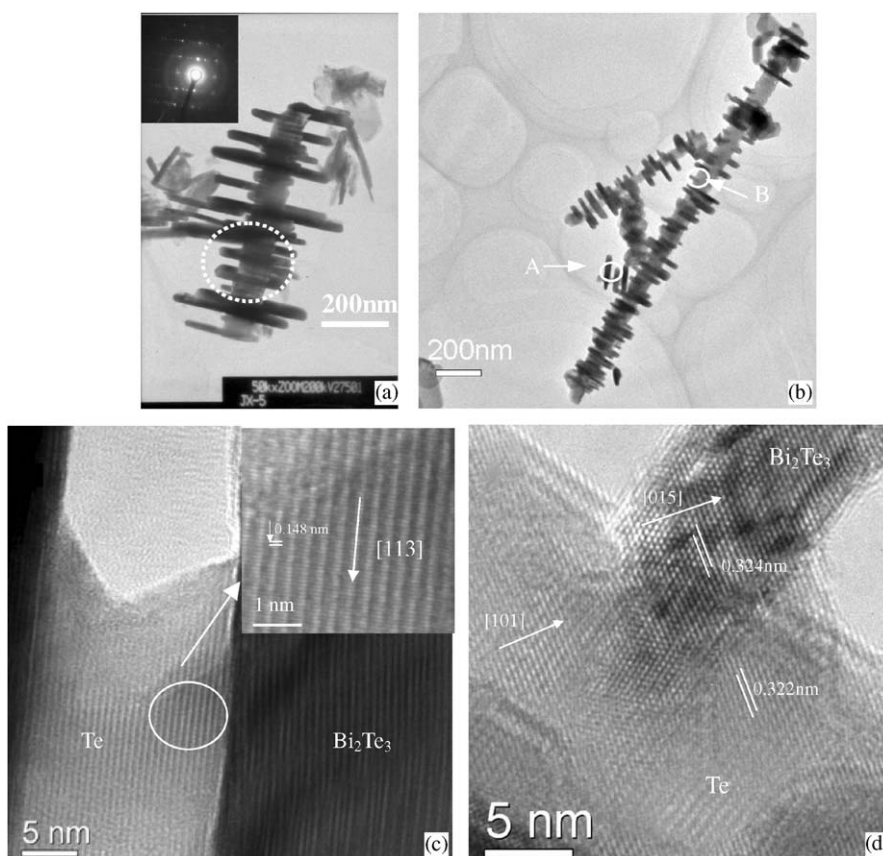


Fig. 3. (a–b) TEM images of the resulting products and SAED patterns recorded from the area enclosed by the dashed circle (inset of a); (c) HRTEM image taken from the area A in b (inset is the enlarged image of the circled areas); (d) HRTEM image taken from the area B in b.

present, implying that the  $c$ -axis of  $\text{Bi}_2\text{Te}_3$  nanosheets is parallel to the  $c$ -axis of the Te rod. As seen from Fig. 3d, the lattice planes in the joint of  $\text{Bi}_2\text{Te}_3$  sheet and Te rod have almost the same spacing and direction, and no apparent boundary is present. It implies that the sheet-rods are composed of epitaxial growth of  $\text{Bi}_2\text{Te}_3$  sheets array on Te rod. The observed fringe pattern of Te rod, with spacing of 0.322 nm, is nicely indexed to the (101) plane of the

hexagonal Te. And the interplanar distance on  $\text{Bi}_2\text{Te}_3$  sheets is 0.324 nm, nearly the same as that of Te rod, which is indexed to the (015) plane of the rhombohedral  $\text{Bi}_2\text{Te}_3$ . A close examination of the lattice reveals that there is a slight misorientation of the lattice fringes between the  $\text{Bi}_2\text{Te}_3$  sheets and the Te rod (about  $1^\circ$ ), as indicated by the white lines in Fig. 3d. Then the lattice is match between the growth direction of Te and  $\text{Bi}_2\text{Te}_3$ . Thus, it is possible to have a

long distance epitaxial growth of  $\text{Bi}_2\text{Te}_3$  on Te, which results in the formation of  $\text{Bi}_2\text{Te}_3$  platelets on Te rod [16].

The synthesis of  $\text{Bi}_2\text{Te}_3$ -Te nanocomposites is a two-step process using Te rods as parent templates. When the Te powders were heated in DMF with KOH at  $180^\circ\text{C}$ , the Te rods appear to form in the initial heating step and then  $\text{Bi}_2\text{Te}_3$  appears to grow epitaxially off the surface of Te rods after they were cooled, added by  $\text{BiCl}_3$  and EDTA and were heated again at  $180^\circ\text{C}$ . If all starting materials were combined in a one-step solvothermal process, it would give  $\text{Bi}_2\text{Te}_3$  sheet-rods [14]. The presence of Te rods at the initial stage of our process is the key point to synthesize  $\text{Bi}_2\text{Te}_3$ -Te sheet-rods. In our reaction process, tellurium powders, DMF and KOH were maintained at  $180^\circ\text{C}$  for 2 h to give Te rods together with some Te particles. Fig. 1c shows the XRD patterns of the Te rods prepared at  $180^\circ\text{C}$  for 2 h. It is identified as a hexagonal Te (JCPDS 36-1452). In contrast to the XRD spectra of Te powders, the intensity of (110) peaks is stronger than normal, indicating that Te rods are preferentially growth along (110) plane. Typical SEM micrograph of as-prepared Te powders is shown in Fig. 4a, which illustrates the tellurium rods have an average width of 100–400 nm and a length up to  $10\ \mu\text{m}$ , and some Te particles are present. TEM image shown in Fig. 4b also proves such a rod-like structure. SAED patterns (see the inset in Fig. 4b) taken from various sites of an individual Te nanorod indicate that Te nanorods synthesized using the present method were crystallized in a single crystalline phase.

The second step is the addition of  $\text{BiCl}_3$  and EDTA to the formed Te rods followed by heating at  $180^\circ\text{C}$  for another 4–30 h,  $\text{Bi}_2\text{Te}_3$  sheets and  $\text{Bi}_2\text{Te}_3$ -Te nanocomposites were found in the final product. At this stage, reaction time has obvious influence on the final chemical composition. When both of the  $\text{BiCl}_3$  and EDTA reacted with the formed Te rods at  $180^\circ\text{C}$  for 4 h, only a few plates, were grown on the surface of the Te rods, proved to be  $\text{Bi}_2\text{Te}_3$  by

EDX analyses as indicated by arrow in Fig. 5a. With the prolongation of reaction time to 10 h, more  $\text{Bi}_2\text{Te}_3$  plates were observed on the surface of the Te rods and some of the  $\text{Bi}_2\text{Te}_3$  plates grew larger (shown in Figs. 5b–d). If the reaction time is prolonged to above 20 h, the  $\text{Bi}_2\text{Te}_3$  plates tend to be around the Te rod (shown in Fig. 5e).

EDTA ligand also plays an important role in the formation of  $\text{Bi}_2\text{Te}_3$ -Te sheet-rods. EDTA acts as not only the coordinating agent of  $\text{Bi}^{3+}$  but also as a soft-template [15]. It is clear that no  $\text{Bi}_2\text{Te}_3$ -Te or  $\text{Bi}_2\text{Te}_3$  sheet-rods were formed in the final product in the absence of EDTA.

The exact mechanism for the formation of the sheet-rod-like nanostructures is still under investigation. According to the images shown in Fig. 5, the  $\text{Bi}_2\text{Te}_3$  sheet-rods in this solvothermal process occur mainly by the following route as a dissolution–precipitation–reaction–growth process to result in such a novel nanostructure. The whole reaction process can be expressed as follow (shown in Fig. 6): in the first step, Te powders are dissolved slowly in KOH and the Te nuclei precipitate from the solution and some of the nuclei quickly grow into Te rods. During the next solvothermal treatment with Bi salt and EDTA, the defects on crystalline Te rods are easy to undergo a reaction with  $\text{Bi}^{3+}$  or  $[\text{Bi}(\text{EDTA})]^+$  to give  $\text{Bi}_2\text{Te}_3$  seeds on Te rods, while the other areas on the surface of Te rods is comparably stable and the reaction occurs slowly. The epitaxial orientation relationship of the growth direction between  $\text{Bi}_2\text{Te}_3$  and Te is preserved to reduce the lattice mismatch energy. The formed  $\text{Bi}_2\text{Te}_3$  seeds tend to grow into the sheet shape under the influence of EDTA [14]. Further epitaxial growth of the  $\text{Bi}_2\text{Te}_3$  seeds perpendicular to the axial direction of the Te rod forms the structure of  $\text{Bi}_2\text{Te}_3$  sheets array. Finally,  $\text{Bi}_2\text{Te}_3$ -Te sheet-rods form the final product. And this facile solvothermal route might also be used as a method of making a new generation of sophisticated nanostructures such as  $\text{Bi}_2\text{Te}_3$ -Te sheet-tube possible, if Te tubes are used as parent templates.

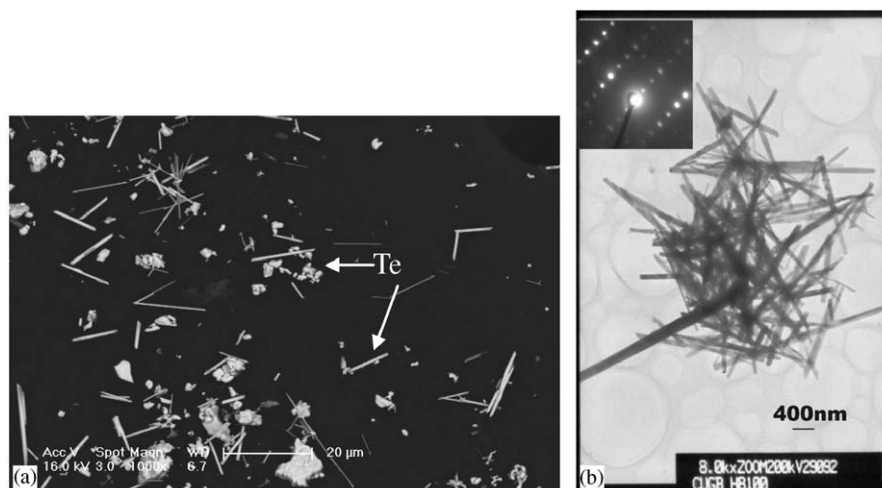


Fig. 4. Micrographs of as-prepared Te powders by the reaction of tellurium powders, DMF and KOH maintained at  $180^\circ\text{C}$  for 2 h (a) SEM image and (b) TEM image with SAED patterns recorded from Te rods.



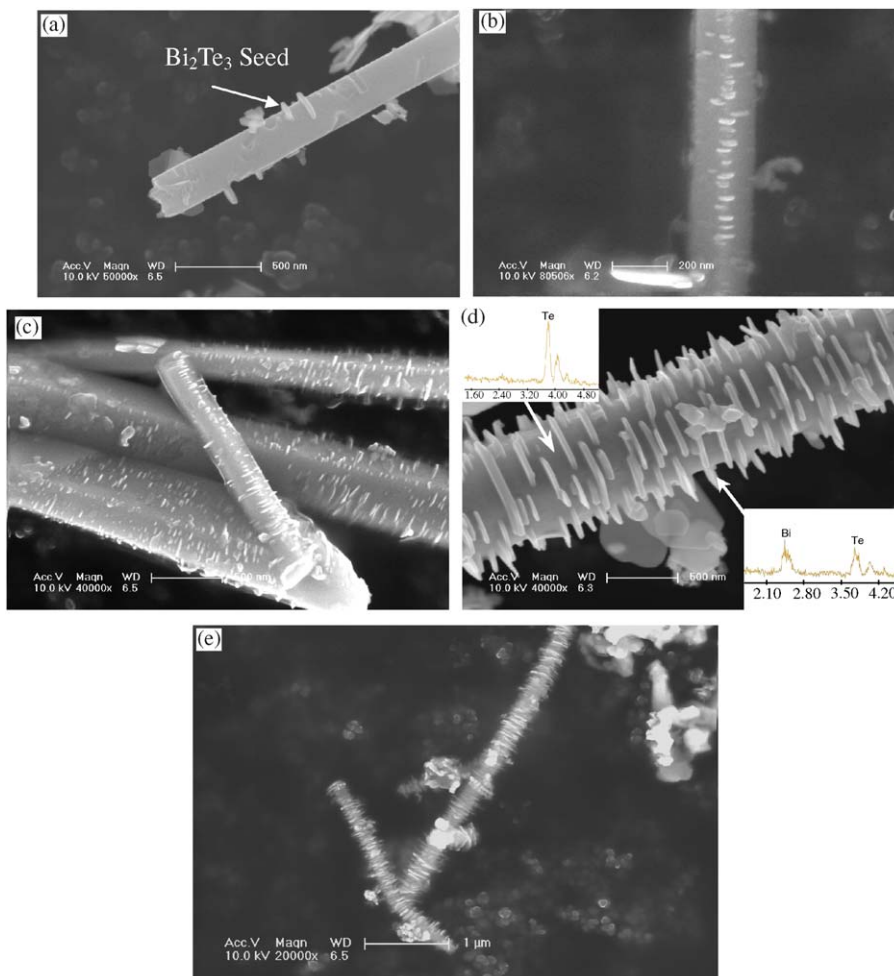


Fig. 5. SEM images of (a)  $\text{Bi}_2\text{Te}_3$ -Te sheet-rods prepared by the reaction of  $\text{BiCl}_3$ , EDTA and the formed Te rods at  $180^\circ\text{C}$  for 4 h; (b–d)  $\text{Bi}_2\text{Te}_3$ -Te sheet-rods prepared by the reaction of  $\text{BiCl}_3$ , EDTA and the formed Te rods at  $180^\circ\text{C}$  for 10 h, and EDX pattern (inset of d) taken from sheet and rod. (e)  $\text{Bi}_2\text{Te}_3$ -Te sheet-rods prepared by the reaction of  $\text{BiCl}_3$ , EDTA and the formed Te rods at  $180^\circ\text{C}$  for 20 h.

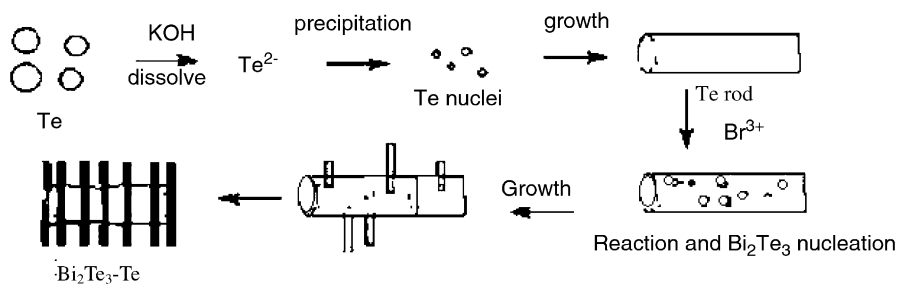


Fig. 6. Proposed growth process of the  $\text{Bi}_2\text{Te}_3$ -Te nanocomposites.

#### 4. Conclusions

In conclusion, single-crystal  $\text{Bi}_2\text{Te}_3$ -Te nanocomposites, with a shape of sheet-rod, have been synthesized by a two-step solvothermal process in the presence of EDTA. The synthesis strategy is using Te rods as parent templates. Te rods are intentionally formed in a first step and  $\text{Bi}_2\text{Te}_3$  forms in a second step off the surface of these rods. Of interest to note is the formation of the  $\text{Bi}_2\text{Te}_3$ -Te

nanocomposites is due to the epitaxial growth of  $\text{Bi}_2\text{Te}_3$  nanosheets off the surface of the Te rod by packing them perpendicular to the axis of the central Te rod. We believe that these well-built structures are desired low-dimensional thermoelectric building-blocks for possibly achieving a high thermoelectric figure of merit. And this facile solvothermal route will be used to make a new generation of sophisticated nanostructures possible, such as  $\text{Bi}_2\text{Te}_3$ -Te sheet-tube.

## Acknowledgments

This work was supported by National Natural Science Foundation of China under Grant no. 50302002 and Beijing Novel Program under Grant no. 2003B06.

## References

- [1] L.D. Hicks, M.S. Dresselhaus, *Phys. Rev. B* 47 (1993) 12727.
- [2] L.D. Hicks, M.S. Dresselhaus, *Phys. Rev. B* 47 (1993) 16631.
- [3] R. Venkatasubramanian, E. Siivola, T. Colpitts, B. O'Quinn, *Nature* 413 (2001) 597.
- [4] K.F. Hsu, S. Loo, F. Guo, W. Chen, J.S. Dyck, C. Uher, T. Hogan, E.K. Polychroniadis, M.G. Kanatzidis, *Science* 303 (2004) 818.
- [5] X.B. Zhao, X.H. Ji, Y.H. Zhang, T.J. Zhu, J.P. Tu, X.B. Zhang, *Appl. Phys. Lett.* 86 (2005) 062111.
- [6] A. Majumdar, *Science* 303 (2004) 777.
- [7] M.S. Toprak, C. Stiewe, D. Platzek, S. Williams, L. Bertini, E. Müller, C. Gatti, Y. Zhang, M. Rowe, M. Muhammed, *Adv. Funct. Mater.* 14 (2004) 1189.
- [8] R. Shenhar, T.B. Norsten, V.M. Rotello, *Adv. Mater.* 17 (2005) 657.
- [9] E. Leontidis, M. Orphanou, T. Kyprianidou-Leodidou, F. Krumeich, W. Caseri, *Nano Lett.* 3 (2003) 569.
- [10] S.A. Sapp, B.B. Lakshmi, C.R. Martin, *Adv. Mater.* 11 (1999) 402.
- [11] A.L. Prieto, M.S. Sander, M.S. Martin-Gonzalez, R. Gronsky, T. Sands, A.M. Stacy, *J. Am. Chem. Soc.* 123 (2001) 7160.
- [12] E.J. Menke, Q. Li, R.M. Penner, *Nano Lett.* 4 (2004) 2004.
- [13] W. Lu, Y. Ding, Y. Chen, Z.L. Wang, J. Fang, *J. Am. Chem. Soc.* 127 (2005) 10112.
- [14] Y. Deng, C.W. Nan, L. Guo, *Chem. Phys. Lett.* 383 (2004) 572.
- [15] Y. Deng, G.D. Wei, C.W. Nan, *Chem. Phys. Lett.* 368 (2003) 639.
- [16] R.L. Penn, G. Oskam, T.J. Strathmann, P.C. Searson, A.T. Stone, D.R. Veblen, *J. Phys. Chem. B* 105 (2001) 2177.